Mon. Not. R. Astron. Soc. **000**, 000–000 (0000) Printed 27 February 2013 (MN LATEX style file v2.2)

Effects of rotation on the Lyman-α line morphology in distant galaxies

Nicolas Garavito-Camargo.[1] Jaime E. Forero-Romero[2]

[1] *Uni A* [2] *Uni B*

27 February 2013

ABSTRACT

Key words: galaxies: high-redshift - galaxies: star formation - line: formation

1 INTRODUCTION

Due to the resonant nature of the lyman alpha line, gas kinematics play an important role shaping its morphology. In the literature there has been extensive studies of outflow/inflow configurations.

In this paper we study for the first time the impact of rotation on the morphology of the Lyman α line. To isolate the effects of rotation we focus on a simple system: the gas distribution is spherical, with homogenous density and the gas rotates as a solid body.

This paper is paper is structured as follows.

2 IMPLEMENTATION OF BULK GAS ROTATION

We implement into CLARA the simplest model whereby a sphere rotates with homogeneous angular velocity. We define a cartesian coordinate system with its origin at the center of the sphere and the rotation axis to be the z-axis, the components in the bulk velocity field, $\vec{v} = v_x\hat{i} + v_y\hat{j} + v_z\hat{k}$. in the gas can be written as

$$v_x = -\frac{y}{R}V_{\rm max}, \tag{1a}$$

$$v_y = \frac{x}{R}V_{\rm max}, \tag{1b}$$

$$v_z = 0, \tag{1c}$$

where R is the radius of the sphere and $V_{\rm max}$ is the linear velocity at the sphere's surface. The minus sign in the x-component of the velocity indicates the direction of rotation, in this case we assume that the angular velocity vector goes in the $\hat{k}$ direction. The linear dependence of the velocity on the radial distance describes the case of constant angular velocity $\omega = V_{\rm max}/R$.

We take the polar angle θ that a unitary vector makes with the rotation axis as defined by the dot product $\cos\theta = \hat{u}\cdot\hat{k}$. In the Section 4 we will present in detail how the line differs at different observing angles θ.

Velocity (km s^{-1})	$V_{\rm max}$	0, 50, 100, 200, 300
Hydrogen Optical Depth	τ_H	10^5, 10^6, 10^7
Dust Optical Depth	τ_A	0,1
Photons Distributions		Central, Homogeneous

Table 1. Values for the varying input parameters in CLARA. Taking into account all the possible combinations for these models

3 GRID OF SIMULATED MODELS

We compute the emergent Lyman-α line for several models with differents values for the maximal rotational velocity, hydrogend optical depth, dust optical depth and initial distributions of the photons with respect to the gas. There are in total 60 models with the input parameters summarized in Table 1.

4 RESULTS

The central result of this paper is summarized in Fig. **??** where we show that rotation has a considerable effect on the morphology of the emergent Lyman-alpha line both in the case where the photons are emitted at the sphere's center and when they are initialized with an homogeneous distribution all over the gas volume.

The results for these outgoing spectra are integrated over the whole sphere, meaning that all the escaping photons were taking into account regardless of the direction of the outgoing photons. Figure **??** shows how if one gives a weight to each outgoing photon according to its direction when escaping the gas distribution it is posible to detect notable differences in the spectrum for different viewing angles.

In the following subsections we quantify the trends observed in Fig. 1 and Fig. 2 as a function of the maximum rotation velocity $V_{\rm max}$ and the position of the observer with respect to the rotation angle, $\mu = \cos\theta$. All the results in this

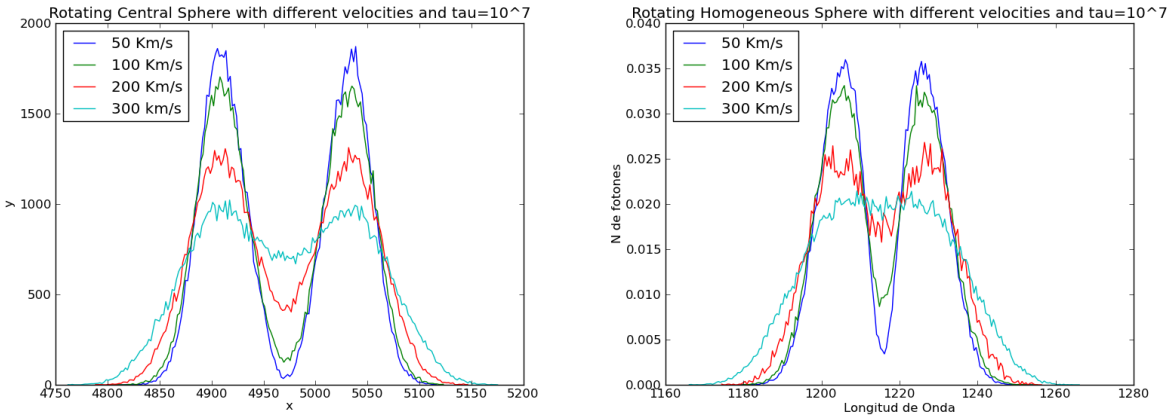

Figure 1. Shape of the lyman alpha line for differents velocities. The left (right) panel shows the central (homogeneous) photon distribution. All photons were taken into account regardless of their outgoing direction of propagation.

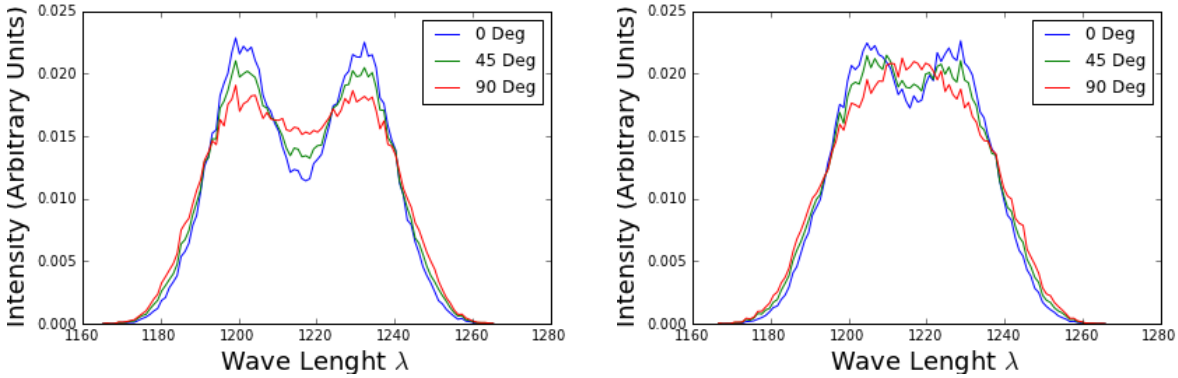

Figure 2. Same as Figure 1 but this time the differen lines show the line morphology for different polar angles θ with respect to the rotation axis. In this case each photon has a weight dependent on their outgoing direction. All spectra correspond to the same $V_{\rm max} = 300\,{\rm km\ s^{-1}}$, Optical Depth $\tau = 10^7$ and Central Distribution without dust.

section will be expressed in terms of frequencies expressed in velocities.

Next, we quantify the line by its full width at half maximum (FWHM) and the peak positions. In the next subsection we take a look at the escape fraction. We conclude the section by estimating the expected line flux for top hat filters at a fixed center and varying width.

4.1 Line width and peak maxima

The first quantitative conclusion of the effect of rotation in the Lyman alpha line is that the double peaks in the line tend to broaden until they reach a single broad emission peak. This is most evident in the case of Lyman-alpha sources homogeneously distributed in the gas distributions (Fig. **??** right panel).

To quantify the line broadening we measure a modified version of the full width at half maximum (FWHM) for half of the line, $W_{1/2}$. It means that in the case of double peaked emission, $W_{1/2}$ corresponds to the with one of thepeaks, while in the extreme case when the line is converted into a single peak, $W_{1/2}$ corresponds to half of the full width.

This definition allows us to quantify the line width both in the cases of double and single peak emission. Furthermore it has the advantage that this line width should have a direct observational correspondence to the observed line feature once the Inter-Galactic Medium (IGM) effects are taken into account, which have the central effect of strongly reducing the intensity of the blue peak of the line.

Figure 3 summarizes our findings for $W_{1/2}$ as a function of $V_{\rm max}$. The line width increases with the rotational velocity of the gas cloud. This increase can be of a factor of $2-3$ with respect to the width with respect to the static case. This trend is conserved at all optical depths regardless of the initial source distribution.

This result includes all the outgoing photons, regardless of the position of the observer. In Figure **??** we take into account the different positions of the observer in the measurement of the half-width $W_{1/2}$. From this we conclude that observers with a line of sight perpendicular to the axis of rotation (i.e. edge-on in the case of spiral galaxy) tend to meaure larger line widths than observers aligned with the rotation axis (i.e. face-on). The influence of the observer position on the line width, amounting always less than 15% of a difference with respect to the result that takes into account

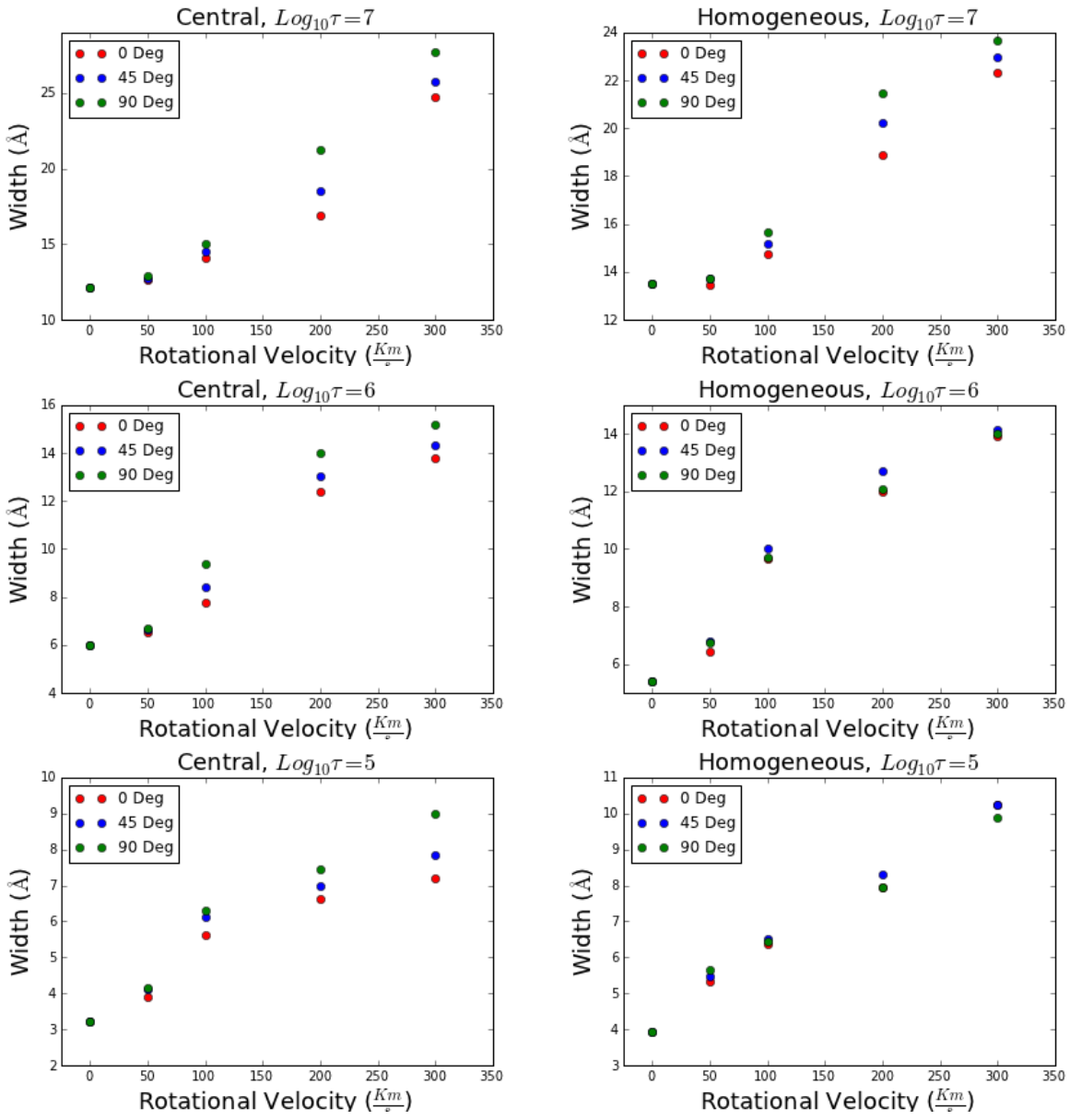

Figure 3. Width of the lyman-alpha line for all the models.

all the outgoing photons with the same weight regardless of the relative observer position.

The second feature in the line that we use to quantify the effect of rotation is the position of the line maxima. These provide information on the wavelength of the majority of the outgoing photons after they interact with the neutral hydrogen atoms in the gas cloud. If most of the photon escapes with a low number of scattering, its outgoing frequency will be close to its initial frequency, that is in the center of the line. On the contrary if the number of scatterings is large for the average photon, its outgoing frequency will be far from the line center. Such reasoning can be made more quantitative to understand the dependence of the peak maxima as a function of the hydrogen optical depth in the cloud [citation needed].

In Figure **??** we present the position of the maxima as a function of $V_{\max}$. For the photons emitted in the line center we do not find any variation in the position of the maxima in the range of explored parameter space. However in the homogeneous case we can see how the maxima goes to $x_m = 0$, meaning that the double peak is converted into a single peak.

This transition to a single peak line occurs for the systems where it becomes easiear for a bulk of the photons to escape with the lowest number of scatterings possible. This can explain how the single peak stage can be achieved in the homogeneous source distribution where there is fraction of the photons inside a photosphere region with $\tau_H \sim 1$ which allows them to escape within one scatter. Increasing the rotational velocity makes it easier for the photons in this photosphere region to escape.

If we now study the effect of the optical depth τ in the maxima position X_m Figure **??**, we found that as the optical depth increase the maximum position increase and

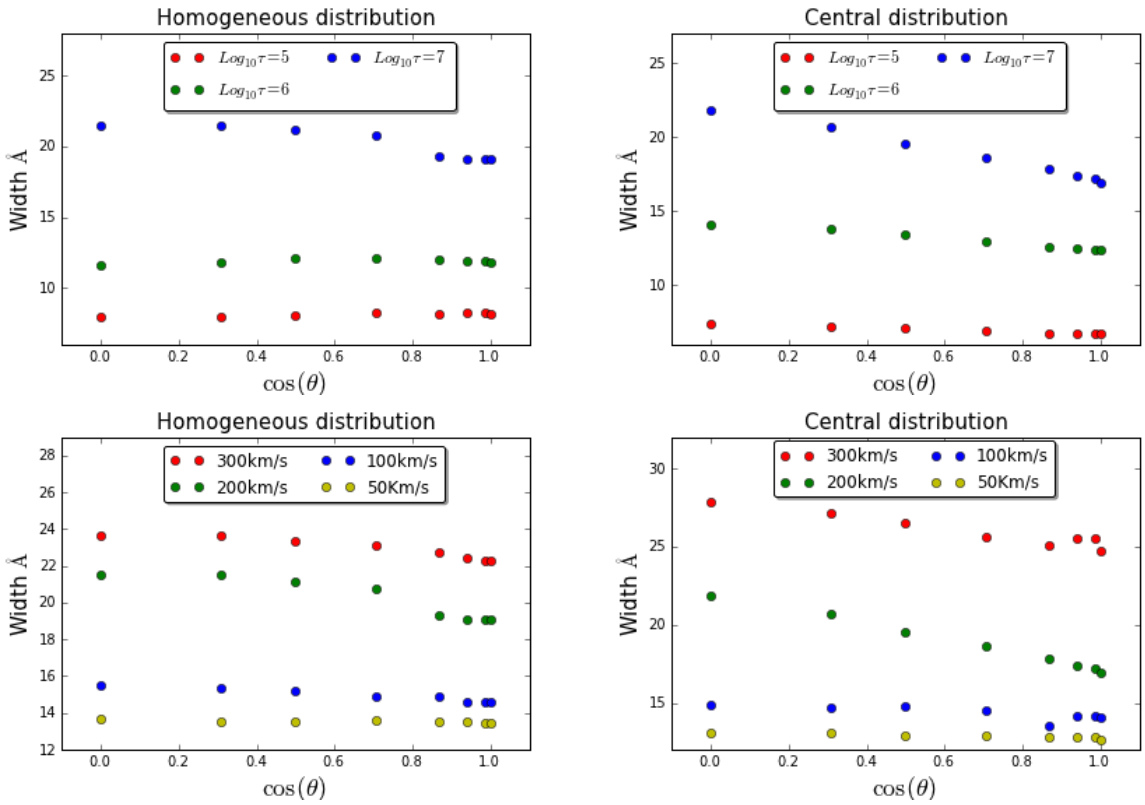

Figure 4. Width of the lyman-alpha line for all the models.

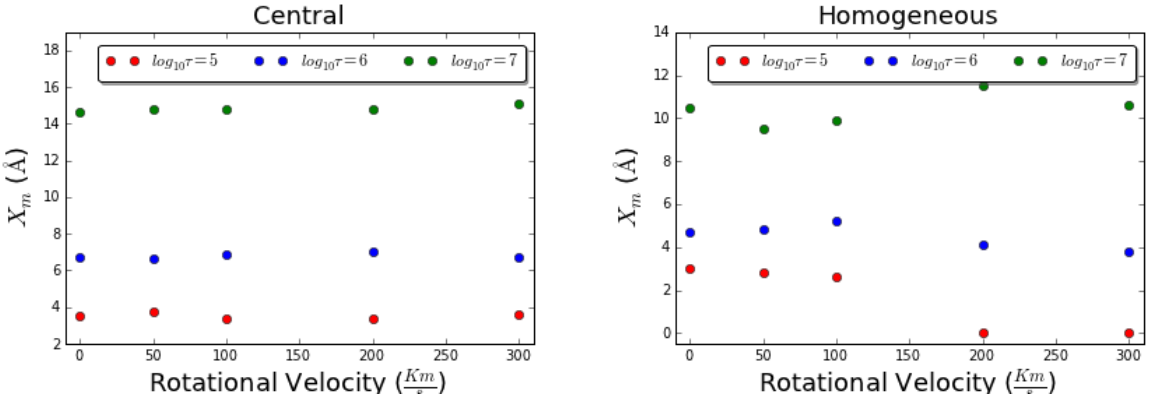

Figure 5. Position of the maxima in the outgoing spectra for differents Rotational velocities, (up)Central Distriution, (Down) Homogeneous Distribution.

this is a well-known result (include references), we found that this result is not modified by rotation.

Finally when we take into account the viewing angle Fig **??** we found that X_m does not depend on it, but again there is a threshold for the homogeneous distribution in which the double peaked merged into a single peak but this time it is just the angle of viewing effect.

4.2 Full Width at Half Maximum of the Lyman alpha line

4.3 Escape Fraction

The fraction of photons that escape from the cloud of gas and dust is defined as:

$$F_e = \frac{\Sigma_{NI}\vec{k}\cdot\vec{o}}{\Sigma_{NF}\vec{k}\cdot\vec{o}} \quad (2)$$

Where NI is the initial number of photons and NF is the final, $\vec{k}$ is the rotation axis direction and $\vec{o}$ the observer

Velocity (Km/s)	Maximum 1 position	Maximum 2 position
50	-16.2695	16.23705
100	-15.66496	15.33504
200	-16.93149	14.56851
300	-13.40048	16.09952

Table 2. Optical Depth $\tau = 10^7$, Central Distribution

Velocity (km/s)	Maximum 1 position	Maximum 2 position
50	-7.46286	6.53714
100	-7.53357	6.96643
200	-8.17453	7.32547
300	-6.81487	6.18513

Table 3. Optical Depth $\tau = 10^6$, Central Distribution

direction. With this definition we compute the escape fraction for all of our models, the results are shown in Fig 4.3

We found that for the central distribution the escape fraction does not depend in velocity neither in the angle of observation, while it does in the optical depth, this result was already known from previous works (references). On the other hand for the homogeneous distribution we found that for higher velocities photons escape easily. The difference between this two results is due to the fact that in the homogeneous distribution photons are emitted closer to the escape surface and this makes this configuration more sensitive to rotation. This last argument also explain the fact that in the homogeneous distribution the optical depth does not affects the escape fraction .

5 DISCUSSION

6 OBSERVATIONAL IMPLICATIONS

... The results derived in this paper have consequences on the interpreation of galaxy observations in the Lyman alpha line.

7 CONCLUSIONS

ACKNOWLEDGEMENTS

APPENDIX A: TABLES

Line width

Velocity(Km/s)	Maximum 1 position	Maximum 2 position
50	-4.33708	3.66292
100	-4.27326	3.72674
200	-3.7737	3.7263
300	-3.84903	4.15097

Table 4. Optical Depth $\tau = 10^5$, Central distribution

Velocity(Km/s)	FWHM	θ
50	12.62	0^o
50	12.72	45^o
50	12.93	90^o
100	14.07	0^o
100	14.48	45^o
100	15.00	90^o
200	16.90	0^o
200	18.51	45^o
200	21.24	90^o
300	24.69*	0^o
300	25.79*	45^o
300	27.73*	90^o

Table 5. Lines Widhts for a Central Distribution and $\tau = 10^7$

[H]

Model	Velocity (km/s)	θ	Dust $\sum(s)$	$\sum(s)$
Homogeneous	50	0^o	13293.06	49939.53
Homogeneous	50	45^o	13291.04	50001.59
Homogeneous	50	90^o	13348.76	49922.73
Homogeneous	100	0^o	15527.69	50114.11
Homogeneous	100	45^o	15511.56	49967.17
Homogeneous	100	90^o	15401.71	49833.65
Homogeneous	200	0^o	17830.85	50078.69
Homogeneous	200	45^o	17932.87	50064.42
Homogeneous	200	90^o	17830.85	49931.748
Homogeneous	300	0^o	18687.33	50048.33
Homogeneous	300	45^o	18572.12	49922.67
Homogeneous	300	90^o	18421.79	49979.37

Table 6. Escape fraction for a Homogeneous Distribution and optical depth 10^5.

Escape fraction

Model	Velocity (km/s)	θ	Dust $\sum(s)$	$\sum(s)$
Central	50	0^o	4809.881	49917.069
Central	50	45^o	4829.21	49811.79
Central	50	90^o	4845.108	49853.039
Central	100	0^o	4809.665	49921.30
Central	100	45^o	4828.65	49820.13
Central	100	90^o	4846.45	49854.0
Central	200	0^o	4809.63	49917.64
Central	200	45^o	4829.25	49818.49
Central	200	90^o	4844.89	49856.66
Central	300	0^o	4810.56	49922.98
Central	300	45^o	4831.16	49823.33
Central	300	90^o	4845.33	49858.48

Table 7. Escape fraction for the central Distribution and optical depth 10^5.

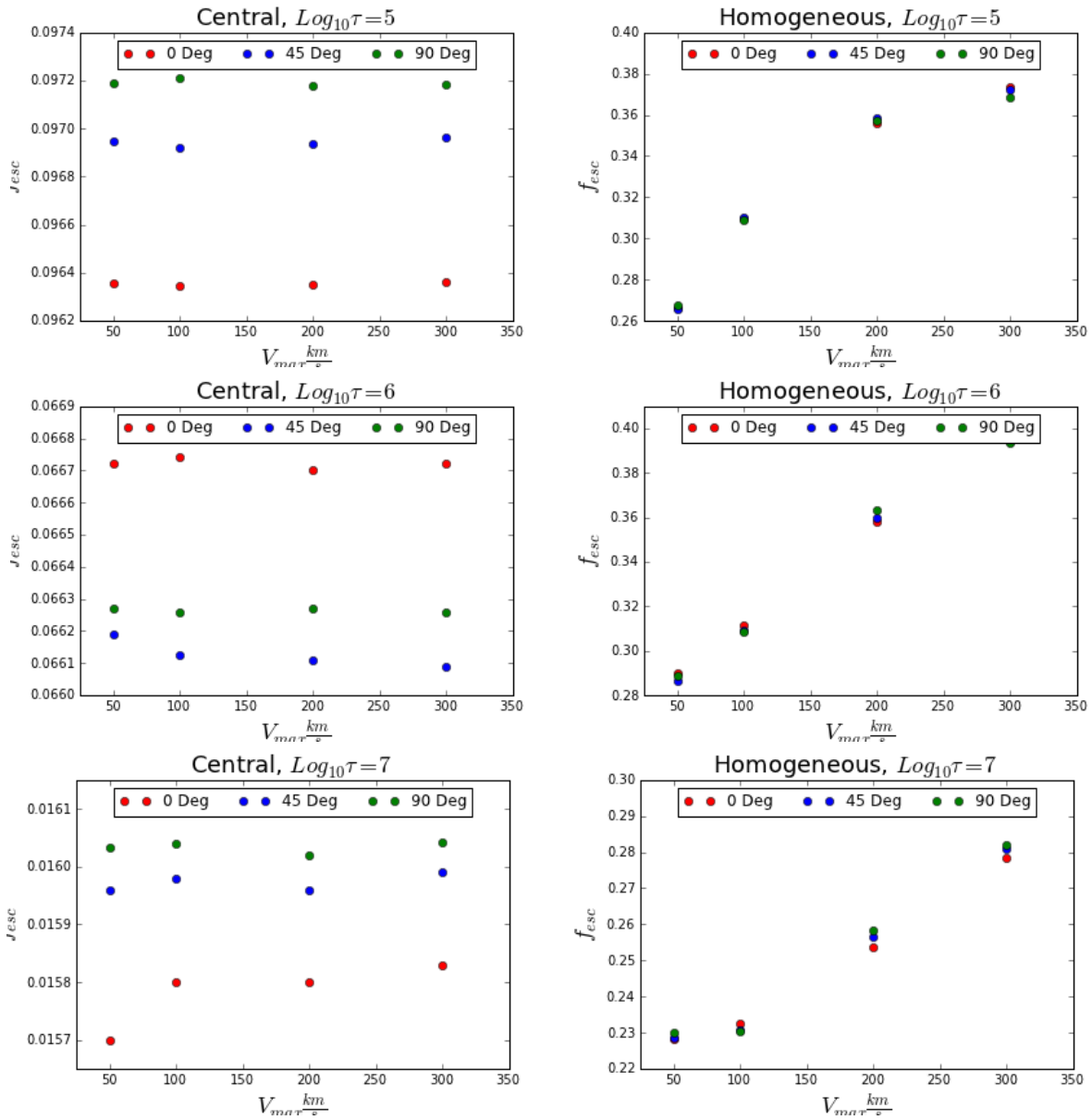

Figure 6. Escape fraction for all the models. Left panels show the central distribution, while right panels show the homogeneous distribution